ACS OMEGA

Open Access

http://pubs.acs.org/journal/acsodf

Article

Dihydroartemisinin-Ursodeoxycholic Bile Acid Hybrids in the Fight against SARS-CoV-2

Elena Marchesi,[#] Valentina Gentili,[#] Daria Bortolotti, Lorenzo Preti, Paolo Marchetti, Virginia Cristofori, Anna Fantinati, Roberta Rizzo, Claudio Trapella, Daniela Perrone,[*,▽] and Maria Luisa Navacchia[*,▽]

Cite This: *ACS Omega* 2023, 8, 45078−45087

Read Online

ACCESS | Metrics & More | Article Recommendations | Supporting Information

ABSTRACT: Here, we propose the molecular hybridization of dihydroartemisinin (DHA) and ursodeoxycholic bile acid (UDCA), approved drugs, for the preparation of antiviral agents against SARS-CoV-2. DHA and UDCA were selected on the basis of their recently demonstrated *in vitro* activity against SARS-CoV-2. A selection of DHA-UDCA-based hybrids obtained by varying the nature of the linkage and the bile acid conjugation point as well as unconjugated DHA and UDCA were tested *in vitro* for cytotoxicity and anti-SARS-CoV-2 activity on Vero E6 and Calu-3 human lung cells. The hybrid DHA-t-UDCMe, obtained by conjugation via click chemistry on a gram scale, was identified as a potential candidate for SARS-CoV-2 infection treatment due to significant reduction of viral replication, possibly involving ACE2 downregulation, no cytotoxicity, and chemical stability.

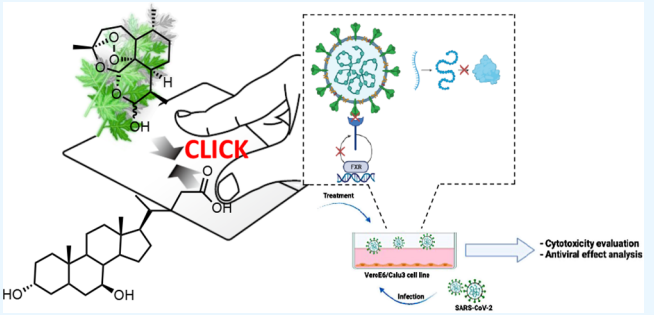

1. INTRODUCTION

The COVID-19 pandemic has dramatically affected the population worldwide, with over 600 million confirmed cases and 6.5 million deaths to date.[1] Moreover, the long COVID sequelae, particularly at the enteric and cardiovascular level,[2−6] compromises the quality of life of millions of people all over the world and burdens on the healthcare systems. Despite the unprecedented speed of vaccine development and global mass vaccination efforts, the appearance of new SARS-CoV-2 variants threatens the effectiveness of existing vaccines; therefore, infected individuals still need treatment options. Among the different therapeutic strategies proposed to counteract SARS-CoV-2 infection, the use of repurposed drugs as antiviral agents reported unsuccessful or discordant results.[7,8] Therefore, the development of small-molecule antivirals against SARS-CoV-2 can provide an important therapeutic treatment option and remains a pressing matter.[9]

Natural products, as well as their structural analogues, represent a very important source of active compounds for pharmacotherapy, especially for cancer and infectious diseases.[10] Artemisinin, obtained from *Artemisia annua*, a plant belonging to the Asteraceae family used in traditional Chinese medicine, is best known as an antimalarial agent.[11] Artemisinin and its derivatives, the so-called artemisinins, in addition to their use as standard therapy for malaria, are known to exert multiple pharmacological activities, including anticancer[12,13] and antiviral effects against several DNA and RNA viruses by affecting viral protein synthesis.[14−17] Based upon data reporting the antiviral potential of antimalarial agents on SARS-CoV-2 infection, artemisinins have been considered as potential candidates against SARS-CoV-2[18] themselves and in combination therapies.[19,20] In particular, it has been recently demonstrated that dihydroartemisinin (DHA) (Figure 1a) represents a possible candidate for SARS-CoV-2 treatment being able to inhibit SARS-CoV-2 replication *in vitro* by decreasing viral protein production.[18] However, a large pharmacological application of artemisinins is limited by the short half-life, poor water solubility, and lack of bioavailability. The development of artemisinin-derived hybrid molecules has been recognized as a valuable approach to overcoming these limitations. Indeed, many studies have been reported on artemisinin-derived hybrids as anticancer[21] and antimalarial[22,23] candidates over the past decade. Molecular hybridization, based on the conjugation of bioactive molecules through covalent bonds, has been recognized to be an efficient tool to improve the stability, activity, selectivity, and safety profile as well as to overcome drug resistance with respect to the components.[24] The new hybrid molecules can also act synergistically and improve upon the simple drug combination.[25]

Received: September 14, 2023
Revised: October 5, 2023
Accepted: October 13, 2023
Published: November 14, 2023

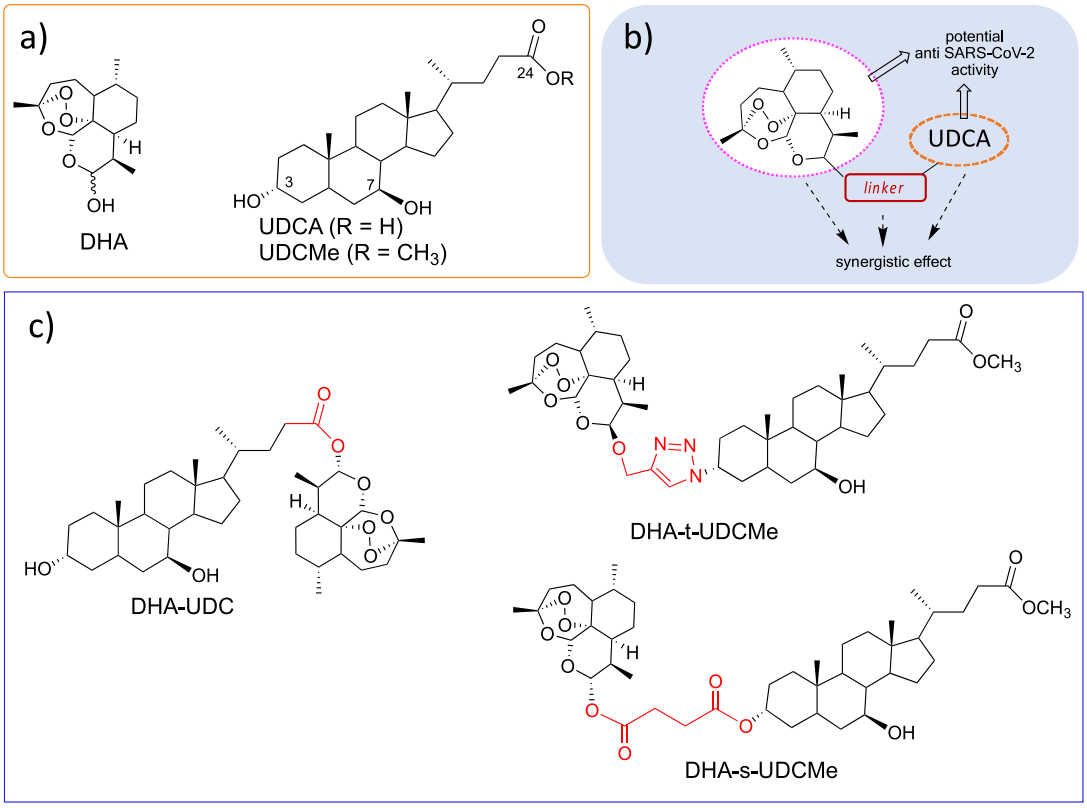

Figure 1. Structure of parent molecules DHA and UDCA (a), sketch of the hybrid molecule (b), and structure of hybrids evaluated in this work (c).

Scheme 1. Synthesis of DHA-t-UDCMe[a]

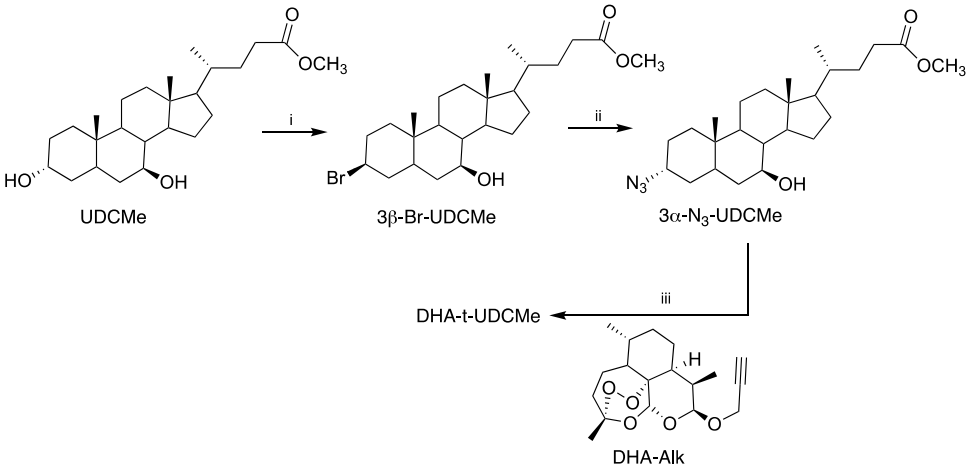

[a](i) NBS, Ph_3P, THF, r.t., 1 h; (ii) NaN_3, DMF, 40 °C, 18 h, 73% two-step yield; (iii) $CuSO_4$, sodium ascorbate, $CH_2Cl_2/H_2O/CH_3CN$ (1:1:0.1), r.t., 1 h, 72% yield.

Bile acids, the major components of bile, apart from their conventional role as surfactants in intestinal solubilization and absorption of lipids, can exhibit important properties toward different cell types. Indeed, bile acids are also considered signaling molecules interacting with different receptors, i.e., the G-protein-coupled bile acid receptor-1 (GPBAR-1, also known as TGR5) and the farnesoid X nuclear receptor (FXR).[26−28] Very recently, Brevini et al. demonstrated that ursodeoxycholic acid (UDCA) (Figure 1a) is able to regulate the FXR receptor, a direct regulator of angiotensin-converting enzyme 2 (ACE2) transcription in multiple COVID-19-affected tissues, down-regulating ACE2 levels, thus reducing susceptibility to SARS-CoV-2 in *ex vivo* experiments.[29] The therapeutic potential of UDCA in the regeneration of the airway epithelium damaged by SARS-CoV-2 has also been successfully investigated.[30] Moreover, the potential of UDCA for the prevention of SARS-CoV-2 infection has been currently under evaluation.[31]

Due to the potential anti-SARS-CoV-2 activity of DHA and UDCA, we reported in the present work a study on the antiviral activity anti-SARS-CoV-2 of DHA-UDCA-based hybrids (Figure 1b). Three DHA-UDCA hybrids depicted in Figure 1c, presenting different linkages or conjugation points,

https://doi.org/10.1021/acsomega.3c07034
ACS Omega 2023, 8, 45078−45087

Table 1. Reaction Conditions Study for the CuAAC Click Reaction

entry[a]	DHA-Alk (equiv)	solvent	catalytic system (equiv)	reaction time (h)	yield (%)[c]
1	1	CH_3CN	CuI (0.1)	18.0	28[d]
2	1	CH_3CN[b]	CuI (0.1)	2.0	39
3	1	CH_3CN:DMSO[b] (1:0.1)	CuI (0.1)	2.0	27
4	0.83	CH_2Cl_2/DIPEA[b]	CuI (0.5)	3.0	0
5	1.1	CH_2Cl_2:H_2O (1:1)	NaAsc (0.5), $CuSO_4$ (0.5)	3.5	25
6	1.1	CH_2Cl_2:H_2O (1:1)[b]	NaAsc (0.15), $CuSO_4$ (0.05)	8.0	18
7	1.1	CH_2Cl_2:H_2O:CH_3CN (1:1:0.1)	NaAsc (0.15), $CuSO_4$ (0.05)	1.0	72

[a]All reactions were carried out at r.t. by employing 1 equiv of 3α-N_3-UDCMe. [b]CH_3CN and CH_2Cl_2 were freshly dried, then degassed by a freeze−pump−thaw method, and employed under an argon atmosphere. [c]Yields obtained after chromatographic purification. [d]Conditions previously reported.[32]

were selected. Among them, DHA-s-UDCMe was newly synthesized, whereas DHA-UDC and DHA-t-UDCMe have previously been explored for anticancer activity in selected cancer cell lines by our group.[32−34]

The idea of expanding the biological area of study of DHA-UDCA-based hybrids was also strengthened by the observation that cancer patients are more susceptible to SARS-CoV-2 infection and to adverse outcomes with higher risk of death than the general population.[35−37] Although the biological interplay between cancer and COVID-19 is not currently fully understood, the development of multitarget bioactive molecules can be a valuable approach. Indeed, some artesunate−quinoline hybrids showing combined anticancer and anti-SARS-CoV-2 activity have recently been reported.[38]

The cytotoxicity and antiviral property of the selected hybrids were assayed on SARS-CoV-2-infected African green monkey epithelial kidney cells, Vero E6, and human epithelial lung cells, Calu-3, both expressing ACE2, with the aim to identify leading candidates for anti-SARS-CoV-2 drug research.

2. RESULTS AND DISCUSSION

2.1. Chemistry. Fused hybrid DHA-UDC (Figure 1c), characterized by a labile ester linkage, was synthesized as we previously reported[32] through a condensation reaction in satisfactory yield and purity. The renewed interest in the DHA-t-UDCMe hybrid (Figure 1c) prompted us to revise the synthetic procedure previously reported by our group[32] via the copper-catalyzed azide−alkyne cycloaddition CuAAC (click chemistry) as subsequently described to obtain the desired compound up to a gram scale (Scheme 1).

Some of the envisaged reactions were already high yielding, although vast improvement was needed in some critical synthetic steps such as the synthesis of 3α-N_3-UDCMe and the CuAAC click reaction. The regioselective and stereospecific introduction of the azide group at the C-3 position of UDCMe was accomplished through a double nucleophilic displacement with retention of configuration following our previously described procedure with some improvements.[39,40] In an effort to simplify and scale up the synthetic procedure, we envisaged to obtain 3β-Br-UDCMe avoiding any protection/deprotection strategy. Briefly, regioselective bromination was achieved by using a mixture of *N*-bromosuccinimide (NBS) and triphenylphosphine (Ph_3P) in tetrahydrofuran (THF) at room temperature for 1 h, in an Appel-type reaction (Scheme 1). After workup, precipitation of the residual triphenylphosphine oxide was performed with magnesium chloride ($MgCl_2$) allowing us to obtain 3β-Br-UDCMe with good purity grade (no 3,7-dibromurated side product was detectable by NMR analysis) and to avoid column chromatography purification.[41]

Finally, the substitution reaction with sodium azide (NaN_3) gave 3α-N_3-UDCMe with an excellent yield without any purification step. Having reached our first goal, we focused on the optimization of the copper(I)-catalyzed azide−alkyne cycloaddition reaction. In order to control DHA sensitivity to reduction conditions,[42] several catalytic conditions and solvents were explored (Table 1) eventually enhancing the click reaction yield from 28[32] up to 72% after chromatographic purification. At first, copper iodide (CuI) was employed as a catalyst in anhydrous acetonitrile (CH_3CN), but this method only afforded a maximum yield of 39% after removal of oxygen from the solvent and the reaction atmosphere (Table 1, entry 2). The addition of 10% dimethyl sulfoxide (DMSO), which could act as a radical scavenger and prevent DHA-Alk degradation, did not improve the yield (Table 1, entry 3). Changing the solvent to dichloromethane (CH_2Cl_2) and adding a base were not beneficial at all, and no product formation was observed (Table 1, entry 4). The use of biphasic catalysis in the presence of copper sulfate ($CuSO_4$) and sodium ascorbate (NaAsc) in commonly used conditions afforded the desired compound in low to moderate yields depending on the reaction time (Table 1, entries 5 and 6). On the contrary, the addition of 10% CH_3CN to the biphasic system greatly improved the yield and diminished the reaction time (Table 1, entry 7). It is noteworthy that under the optimized conditions, very little degradation of the DHA-Alk starting material took place. Since it is reported that artemisinin can degrade in the presence of ferrous ion, Fe(II)-heme, or biological reductants,[43,44] we speculated that the presence of copper(I), which is essential for CuAAC catalysis, could also bring about the cleavage of the endoperoxide bridge in DHA-Alk under reductive conditions as previously reported by others.[42] With this in mind, we also speculated that the optimized conditions (Table 1, entry 7) allowed reaching a higher yield due to the faster reaction rate of the click with respect to the degradation reaction. The click reaction performed by employing the conditions reported in Table 1, entry 7 allowed one gram of hybrid DHA-t-UDCMe to be obtained per batch.

The synthesis of DHA-s-UDCMe (Scheme 2), which presents the DHA moiety conjugated at the 3-α-OH position of UDCMe through a succinic linker, has not been reported yet. This compound, although not necessarily a structural analogue of DHA-t-UDCMe, has a labile ester linker between the two conjugation partners instead of the stable triazole moiety and could help elucidate the influence of the linker stability on the antiviral activity of the hybrid. The synthesis of DHA-s-UDCMe was straightforward: having obtained artesunate (ART) by following literature procedures,[45] the

https://doi.org/10.1021/acsomega.3c07034
ACS Omega 2023, 8, 45078−45087

Scheme 2. Synthesis of DHA-s-UDCMe[a]

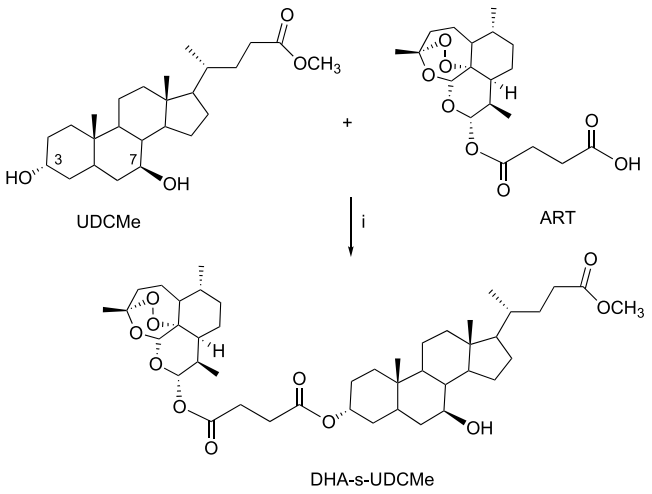

[a](i) EDCI, DMAP, CH_2Cl_2, r.t., 18 h, 48% yield.

esterification with UDCMe gave the desired product in 48% yield.

2.2. Chemical Stability in Cell Culture Medium. Chemical stability of DHA-s-UDCMe in the cell culture medium at 37 °C was established by means of HPLC-MS analyses. A time course of 2, 6, 15, and 24 h demonstrated that hybrid DHA-s-UDCMe underwent decomposition showing a half-life time of ca. 15 h. Hybrids DHA-UDC and DHA-t-UDCMe, previously studied under comparable conditions,[33,34] were found stable up to 24 h of incubation in cell culture medium, whereas the parent DHA was found far more unstable, being decomposed up to 70% after 6 h (Figure 2).[33]

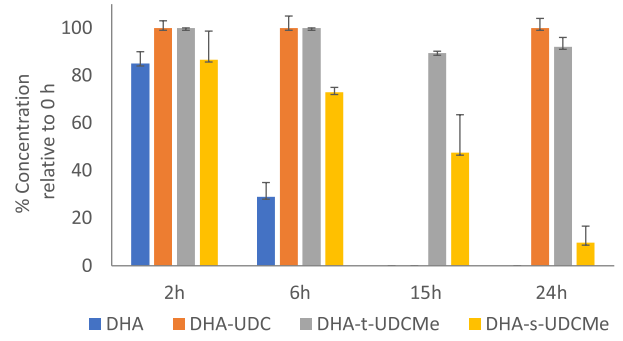

Figure 2. Stability of DHA and DHA-UDCA-based hybrids in cell culture medium assessed by HPLC-MS analyses. Stability of DHA and hybrid DHA-UDC was reported in ref 33; stability of hybrid DHA-t-UDCMe was reported in ref 34; stability of DHA-s-UDCMe was recorded at 3, 6, 15, and 24 h. The data are presented as the mean ± SD of three independent experiments.

The overall data indicated that the molecular hybridization actually improved the chemical stability with respect to the parent DHA although to a lesser extent in the case of hybrid DHA-s-UDCMe, which underwent decomposition up to 80% after 24 h.

2.3. Biological Evaluation. The antiviral properties of all selected hybrids were assayed on SARS-CoV-2-infected Vero E6 and human lung adenocarcinoma Calu-3 cells after cytotoxicity evaluation with the aim to identify leading candidates for anti-SARS-CoV-2 drug research.

The selected hybrids were first tested on the Vero E6 cell line for their anti-SARS-CoV-2 activity along with their cytotoxicity. Vero E6 cells represent a suitable basis for performing the initial screening of antiviral compounds since they are highly susceptible and permissive to SARS-CoV-2 and support viral replication to high titers.[46] Among the hybrids, DHA-t-UDCMe and DHA-s-UDCMe showed the best safety profile with $IC_{50} \gg 100$ μM, whereas UDC-DHA showed an IC_{50} of ca. 100 μM (Figure S1, SI). It is worth noting that all hybrids showed a far higher IC_{50} with respect to DHA (IC_{50} = 21.6 μM); therefore, the molecular hybridization was effective in improving the safety profile with respect to unconjugated DHA (Figure S1, SI). On the other hand, UDCA was found to be noncytotoxic within the concentration range tested as expected (Figure S1, SI). In light of the cytotoxicity results, all the compounds were tested for their antiviral activity at 1 and 10 μM. Infected Vero E6 cells were treated with the proper hybrid, and the results were compared with the antiviral effect of the parent molecules DHA and UDCA. Moreover, to investigate which stage of the virus life cycle was affected by treatment, a time-of-drug addition assay was performed by treating virus-infected cells at specific time points: pre-, during, or postinfection, for 1 h. The viral titer was measured by RT-qPCR of 100 μL of extracted supernatants 48 h postinfection (hpi), and reductions of viral load (LR) more than 1 log were considered effective, corresponding to a 90% decrease.

DHA-UDC and DHA-t-UDCMe hybrids were found to be more effective than unconjugated DHA and UDCA at 10 μM (Figure 3a−e). In particular, hybrid DHA-t-UDCMe was the most effective compound in decreasing the SARS-CoV-2 load in a dose-dependent manner at all stages of viral infection (Figure 3d), with LR > 2.5 in pre- and co-infection phases and LR = 4.97 when administered postinfection (Figure 3e; $p < 0.0001$, Student's t test). Hybrid DHA-UDC exhibited the best effect on the preinfection phase with LR = 1.84, whereas unconjugated DHA and UDCA showed LR < 1 in all stages of the infection (Figure 3e). These results highlight the effectiveness of the molecular hybridization and suggest that interference with the virus entry phase is the main mechanism of action (Figure 3e). In turn, hybrid DHA-s-UDCMe exhibited no significant inhibition of SARS-CoV-2 replication, reporting LR values lower than 1 (data not shown).

The collected data showed the effectiveness of DHA hybridization with UDCA in reducing the toxicity and enhancing the antiviral activity in the case of DHA-UDC and DHA-t-UDCMe hybrids.

In order to confirm the results, the antiviral activity against COVID-19 of DHA-UDC and DHA-t-UDCMe hybrids was further evaluated in Calu-3 cells chosen as a representative human cell model for SARS-CoV-2 infection. DHA-UDC and DHA-t-UDCMe hybrids as well as unconjugated DHA were found to be noncytotoxic toward Calu-3 at a concentration up to 20 μM while slightly altering cell viability at the higher concentrations tested (Figure S2, SI; $p < 0.05$ and $p < 0.01$; Student's t test). On these bases, the evaluation of antiviral activity was performed at 1−10−20 μM.

Hybrid DHA-UDC was found to decrease the viral load in a dose-dependent manner reaching the highest activity (LR = 1.50) if added before infection at 20 μM, in a similar way to that observed in Vero E6 cells (Figure S3, SI; $p < 0.0001$, Student's t test). Hybrid DHA-t-UDCMe presented a different antiviral activity according to the time of addition. Indeed, the infection was significantly reduced in pre- and co-infection

https://doi.org/10.1021/acsomega.3c07034
ACS Omega 2023, 8, 45078−45087

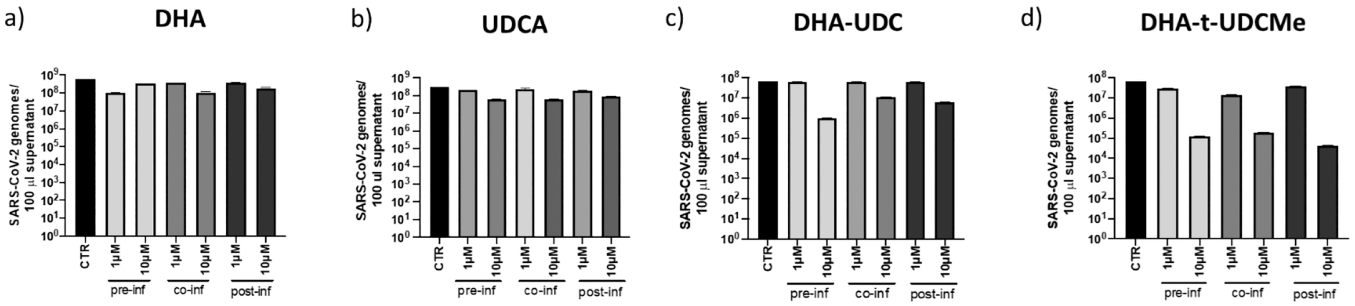

e)

		LR vs Untreated			
Time of drug addition	Concentration	DHA	UDCA	DHA-UDC	DHA-t-UDCMe
Pre-inf	1µM	0.75	0.19	0.03	0.37
	10µM	0.23	0.71	1.84*	2.74*
Co-inf	1µM	0.20	0.13	0.02	0.68
	10µM	0.74	0.69	0.79	2.55*
Post-inf	1µM	0.20	0.23	0.02	0.24
	10µM	0.50	0.56	1.04	4.97*

Figure 3. Evaluation of antiviral activity of compounds DHA, UDCA, DHA-UDC, and DHA-t-UDCMe in Vero E6 SARS-CoV-2-infected cells by RT-qPCR (a–d). Experiments were run in triplicates. Data were reported also as mean log reduction (LR) ± SD in comparison to untreated Vero E6 cells infected with SARS-CoV-2 (e). *Antiviral LR, greater than 1 log, corresponding to a >90% viral load decrease.

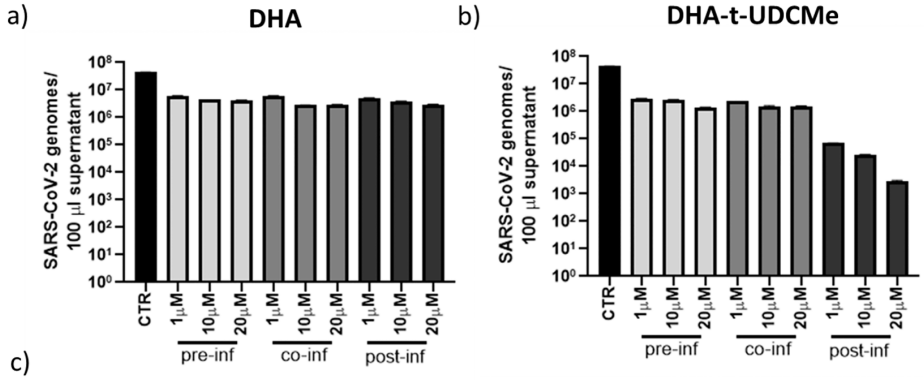

c)

		DHA		DHA-t-UDCMe	
Time of drug addition	Concentration	PFU/100µl supernatant	Log Reduction vs Untreated	PFU/100µl supernatant	Log Reduction vs Untreated
Untreated		44275	-	44275	-
pre-inf	1µM	4673,9	**0,98**	1610	**1,44***
	10µM	5428,5	**0,91**	2695	**1,22***
	20µM	4342,8	**1,01***	2765	**1,20***
co-inf	1µM	3834,6	**1,06***	1665	**1,42***
	10µM	2810,5	**1,19***	1675	**1,42***
	20µM	2895,2	**1,18***	2110	**1,32***
post-inf	1µM	3010,7	**1,18***	80,5	**2,74***
	10µM	4050,2	**1,04***	26,5	**3,22***
	20µM	3803,8	**1,07***	4	**4,04***

Figure 4. Evaluation of antiviral activity of compounds DHA and DHA-t-UDCMe on Calu-3 SARS-CoV-2-infected cells by RT-qPCR (a,b). Data were reported also as viral genome log reduction (LR) and PFU/100 mL supernatant by the plaque assay, in comparison to untreated Calu-3 infected with SARS-CoV-2 (c). Experiments were run in triplicates and reported as means ± SD. *Antiviral LR, greater than 1 log, corresponding to a >90% viral load decrease.

https://doi.org/10.1021/acsomega.3c07034
ACS Omega 2023, 8, 45078−45087

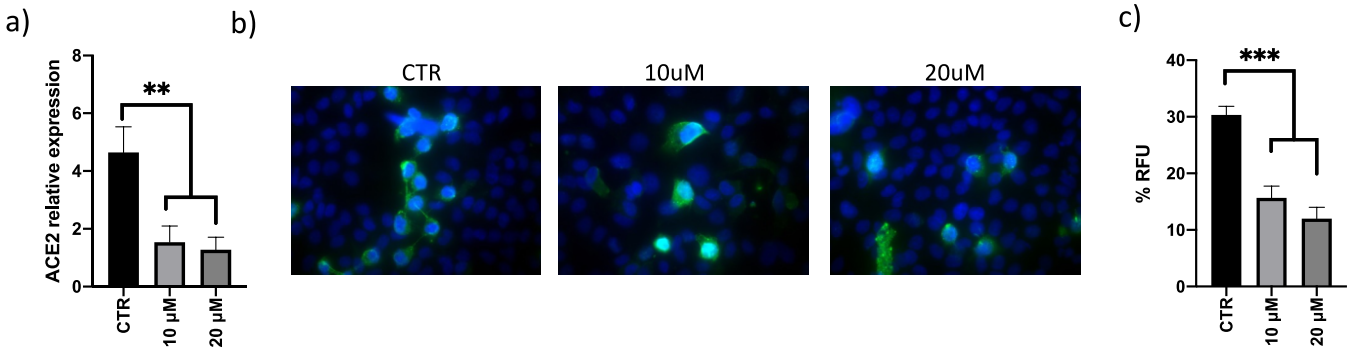

Figure 5. ACE2 expression evaluation in SARS-CoV-2-infected Calu-3 cells after postinfection treatment with hybrid DHA-t-UDCMe at 10 and 20 μM at mRNA (a) and protein level by IF (b,c). RFU: relative fluorescent units.

stages, with LR > 1.2 and 1.4, respectively, but the best activity was reached with postinfection treatment, with LR = 4.04 at 20 μM, when compared with untreated infected cells (Figure 4b,c; $p < 0.0001$, Student's t test) as confirmed by the plaque assay (Figure 4c). Conversely, unconjugated DHA was found to slightly interfere with viral replication independently of the time of administration (Figure 4a,c).

Based on these results, postinfection treatment with compound DHA-t-UDCMe was selected for further investigation.

Since SARS-CoV-2 infection requires the interaction between viral spike protein and the cellular ACE2 receptor to allow viral entry and spread, the postinfection treatment with compound DHA-t-UDCMe was selected to assess the effect on ACE2 expression, in order to determine if the significant reduction of viral replication was consistent with this mechanism. As expected, the infection induced upregulation of ACE2 expression at both the mRNA (Figure 5a) and protein (Figure 5b,c) level. In contrast, postinfection treatment with 10−20 μM hybrid DHA-t-UDCMe led to a significant decrease of ACE2 expression in infected cells, in a dose-dependent manner at both the transcriptional (Figure 5a; $p < 0.01$, Student's t test) and translational level (Figure 5b,c; $p < 0.001$, Student's t test). This result suggests that the reduction of SARS-CoV-2 infection, observed after postinfection treatment with DHA-t-UDCMe, may be due to lower levels of ACE2 availability on the cell surface possibly via FXR inhibition, which reduces the spike-ACE2 interaction rate, interfering with viral entry into the cells. A recently published study demonstrated that UDCA can act as an FXR inhibitor, a known ACE2 regulation factor, decreasing ACE2 expression.[29] Therefore, we can speculate that DHA-t-UDCMe may also affect ACE2 expression via FXR inhibition, even though other mechanisms of action cannot be excluded.

3. CONCLUSIONS

The synthesis of the new hybrid DHA-s-UDCMe was reported, and the optimization of the synthetic procedure for DHA-t-UDCMe, which involves the copper-catalyzed azide−alkyne cycloaddition (CuAAC), has been revised to obtain the desired compound in gram-scale quantities. Both hybrids together with the previously reported DHA-UDC[32] were selected to test *in vitro* their potential antiviral activity against SARS-CoV-2. The DHA-UDC fused hybrid presents the DHA unit directly condensed through a cleavable ester bond to the C-24 position of UDCA allowing both the 3α and 7β hydroxyl groups to be free. The DHA-t-UDCMe hybrid presents the DHA unit covalently linked to the C-3 position of UDCMe through the stable triazole linker. Analogously, the DHA-s-UDCMe hybrid presents a residue of DHA covalently linked to the 3α-OH of UDCMe; however, in this case, a cleavable succinyl linker has been chosen. Both hybrids DHA-UDC and DHA-t-UDCMe were found stable up to 24 h of incubation in cell culture medium independently on the nature of the linkage/linker and the conjugation point,[33,34] whereas hybrid DHA-s-UDCMe showed a half-life time of around 15 h of incubation. All hybrids considered were found markedly more stable than unconjugated DHA that underwent decomposition up to 70% after 6 h of incubation time (Figure 2).[33] Therefore, the hybridization allowed to overcome the chemical instability of DHA in all cases even though to a lesser extent in the case of hybrid DHA-s-UDCMe. The greater chemical stability in cell culture medium of hybrids DHA-UDC and DHA-t-UDCMe with respect to unconjugated DHA may in part account for their marked improved antiviral activity. The greater antiviral activity displayed by hybrid DHA-t-UDCMe with respect to fused hybrid DHA-UDC may be attributable, in part, to the presence of the triazole ring. Indeed, the linker can also play a role in the biological activity of the hybrids.[21] In particular, the triazole moiety is known to improve pharmacological, pharmacokinetic, and physiochemical profiles of active compounds,[47] being somehow considered a pharmacophore itself.

In summary, the *in vitro* study herein reported on both Vero E6 and Calu-3 cell lines revealed DHA-t-UDCMe as a potential candidate for postinfection treatment of SARS-CoV-2 infection due to significant reduction of viral replication, no cytotoxicity, and chemical stability. This outcome could be ascribable to effects on ACE2 regulation, possibly via FXR inhibition as suggested by others,[29] even if further experiments are needed to confirm this hypothesis. The improved synthetic procedure for DHA-t-UDCMe ensures the availability of the hybrid in gram-scale quantities, empowering further essential studies for drug development.

4. EXPERIMENTAL SECTION

4.1. Synthesis and Characterization. *4.1.1. General.* Commercial dihydroartemisinin (DHA) and 1-(3-dimethylaminopropyl)-3-etlylcarbodiimide hydrochloride (EDCI) were purchased from Carbosynth (Compton, Berkshire, UK). Ursodeoxycholic bile acid (UDCA) was kindly furnished by ICE SpA (Reggio Emilia, Italy). Sodium azide (NaN_3), sodium ascorbate (NaAsc), triphenylphosphine (PPh_3), propargylic alcohol, and *N*-bromosuccinimide (NBS) were purchased from

https://doi.org/10.1021/acsomega.3c07034
ACS Omega 2023, 8, 45078−45087

Sigma-Aldrich (St. Louis, MO, USA); copper sulfate pentahydrate ($CuSO_4·5H_2O$) was purchased from Fluka (Buchs, Switzerland); imidazole was obtained from Acros (Geel, Belgium). All of the chemicals were used without further purification. The reactions were monitored by TLC on precoated silica gel F_{254} plates (thickness, 0.25 mm; Merck), developed with phosphomolybdic acid solution. Flash column chromatography was performed on silica gel (60 a, 230−400 mesh). NMR spectra were recorded with a Varian Mercury 400 MHz instrument or a Varian Mercury 300 MHz instrument in the stated solvent. Preparative and analytical HPLC was executed on an XTerra C18 column with a mobile phase composed of water and CH_3CN in gradient at room temperature. Anhydrous solvents were freshly distilled on sodium/benzophenone with standard procedures or purchased anhydrous.

4.1.2. Synthesis of 3β-Br-UDCMe. UDCMe (4.00 g, 9.8 mmol) and PPh_3 (3.85 g, 14.7 mmol) were added to a two-neck 100 mL round-bottom flask equipped with a thermometer. Anhydrous THF (20 mL) was added, and the solution was stirred until dissolution of the solids was achieved. The solution temperature was lowered up to 0 °C and NBS (2.61 g, 14.7 mmol) was added three times. After 5 min, the flask was allowed to reach room temperature. The solution was stirred for 60 min, and then, the reaction was quenched by addition of 10% H_2O_2 solution (30 mL). After 10 min of stirring, the solvent was removed under vacuum. The resulting gummy reddish solid was dissolved in 50 mL of CH_2Cl_2, and the organic phase was washed five times with 10 mL of 10% $Na_2S_2O_5$ solution to remove excess bromine. The clear organic phase was dried by addition of Na_2SO_4, filtered, and the solvent removed under vacuum up to10 mL of solution. $MgCl_2$ (2.83 g, 29.8 mmol) was added to the solution and the resulting mixture was stirred overnight and then filtered on silica to afford, after solvent removal, 3.40 g of the product as a yellowish oil in 74% yield.

^{1}H NMR (300 MHz, $CDCl_3$): δ 4.73 (s, 1H), 3.68 (s, 3H), 3.56−3.29 (m, 1H), 2.44−1.05 (m, 28H), 1.03 (s, 3H), 0.92 (d, J = 6.3 Hz, 3H), 0.68 (s, 3H). ^{13}C NMR (101 MHz, $CDCl_3$): δ 175.15, 72.11, 56.29, 56.09, 55.42, 51.97, 44.23, 44.15, 40.60, 40.10, 38.42, 36.60, 35.73, 35.31, 31.54, 31.50, 31.05, 30.00, 29.06, 27.33, 24.15, 21.74, 18.86, 12.61. HRMS ESI (+) $C_{25}H_{41}BrO_3$: 469.2158 $[M + H]^+$, 491.2189 $[M + Na]^+$.

4.1.3. Synthesis of 3α-N$_3$-UDCMe. NaN_3 (1.41 g, 21.7 mmol) was added to a solution of 3β-Br-UDCMe (3.40 g, 7.25 mmol) in 40 mL of DMF. The reaction mixture was stirred at 40 °C overnight; then, 50 mL of diethyl ether was added, and the organic phase was washed four times with 25 mL of H_2O and once with 25 mL of LiCl saturated aqueous solution. After removal of the solvent, the product was achieved in a quantitative yield. IR, ^{1}H NMR, and ^{13}C NMR spectroscopic data were in agreement with the literature.[39]

4.1.4. Synthesis of DHA-t-UDCMe in Optimized Conditions. 3α-N_3-UDCMe (1.047 g, 2.427 mmol) and DHA-ALK (0.861 g, 2.670 mmol) were dissolved in 22 mL of $CH_2Cl_2/H_2O/CH_3CN$ (1:1:0.1) solution; then 0.73 mL of a 0.5 M solution of NaAsc and 1.21 mL of a 0.1 M $CuSO_4$ solution were added under nitrogen. After 1 h stirring, the reaction mixture was poured into 50 mL of H_2O and extracted with 50 mL of CH_2Cl_2. The organic phase was dried with anhydrous Na_2SO_4, and the solvent was removed under vacuum. The crude product was then purified by flash chromatography (EtOAc/Cy 1:1) to give 1.32g of the product as a white powder in 72% yield. Analytical and spectroscopic data were in agreement with the literature.[32]

^{1}H NMR (400 MHz, $CDCl_3$): δ 7.54 (1H, s), 5.38 (1H, s), 4.94−4.86 (2H, m), 4.72 (1H, d, J = 12.6 Hz), 4.47−4.33 (1H, m), 3.66 (3H, s), 3.64−3.55 (1H, m), 2.68−2.57 (1H, m), 2.47−1.04 (40H, m), 1.03 (3H, s), 0.96−0.90 (6H, m), 0.87 (3H, d, J = 7.2 Hz), 0.69 (3H, s). ^{13}C NMR (101 MHz, $CDCl_3$): δ 174.65, 144.43, 120.60, 104.09, 101.32, 87.81, 80.96, 71.06, 61.51, 60.63, 55.54, 54.87, 52.50, 51.49, 44.37, 43.74, 43.11, 39.92, 39.29, 37.38, 36.49, 35.22, 34.74, 34.57, 31.04, 30.82, 28.54, 28.04, 26.18, 24.42, 23.49, 20.32, 18.38. HRMS ESI (+) $C_{43}H_{67}N_3O_3$: calculated 754.50009 $[M + H]^+$, found: 754.4992 $[M + H]^+$.

4.1.5. Synthesis of DHA-s-UDCMe. Artesunate (ART) was obtained from DHA and purified as described by Presser et al.[45] UDCMe (0.10 g, 0.246 mmol), ART (0.19 g, 0.492 mmol), DMAP (0.02 g, 0.172 mmol) and EDCI (0.09 g, 0.492 mmol) were solved in 10 mL of dry CH_2Cl_2 under nitrogen. The reaction mixture was stirred at room temperature for 18 h, then diluted with 60 mL of CH_2Cl_2 and washed three times with 20 mL of saturated solution of NH_4Cl each and 20 mL of brine. The organic phase was dried with anhydrous Na_2SO_4, and the solvent was evaporated under vacuum to obtain a crude mixture. The white solid was purified by silica gel column chromatography (Cy/EtOAc 7:4) to obtain 0.09 g of DHA-s-UDCMe in a 48% yield. The product was further purified by RP-HPLC on a C18 column. HPLC conditions: Xterra C18 column, CH_3CN/H_2O 10:90 to 90:10 in 15 min, t_r = 15.9 min.

DHA-s-UDCMe: ^{1}H NMR (300 MHz, $CDCl_3$) selected data: δ 5.80 (d, J = 9.9 Hz, 1H), 5.44 (s, 1H), 4.79−4.56 (m, 1H), 3.66 (s, 3H), 3.64−3.49 (m, 1H), 2.81−2.66 (m, 2H), 2.66−2.47 (m, 3H), 2.44−2.30 (m, 2H), 2.29−2.14 (m, 1H), 1.43 (s, 3H), 0.94 (m, 3 CH_3), 0.85 (d, J = 7.1 Hz, CH_3), 0.67 (s, CH_3). ^{13}C NMR (75 MHz, $CDCl_3$): δ 175.06, 171.89, 171.49, 104.80, 92.47, 91.85, 80.46, 74.70, 74.53, 71.58, 56.01, 55.26, 51.89, 45.57, 44.06, 42.60, 40.41, 39.50, 37.61, 36.92, 36.56, 35.59, 34.94, 34.43, 33.39, 32.17, 31.39, 29.62, 29.57, 28.93, 27.19, 26.76, 26.30, 24.92, 23.67, 22.35, 21.54, 20.55, 18.74, 12.47. HRMS ESI (+) $C_{44}H_{68}O_{11}$: 773.4829 $[M + H]^+$, 790.5095 $[M + NH_4]^+$, 795.4646 $[M + Na]^+$.

4.2. Chemical Stability of Hybrid DHA-s-UDCMe. A DMSO mother solution of the DHA-s-UDCMe hybrid at a 20 mM concentration was prepared. The solution was diluted in complete cell culture medium Eagle's minimal essential medium (MEM) to a final concentration of 20 μM. A time course of 0, 2, 6, 15, and 24 h was considered. The solution of each hybrid was analyzed by HPLC-MS, and the concentration of the hybrid during that time was calculated by comparison with that of the initial solution (time 0). The experiment was performed in triplicate (RSD < 10%).

HPLC-MS/MS analyses were performed on a Dyonex Ultimate 3000 HPLC (Thermo Fisher Scientific, Italy) equipped with a triple-quadrupole mass spectrometer TSQ Quantum Access Max and an electrospray ionization source detector; 0.5 mL samples were used as sources for the automated injection. LC-MS-grade acetonitrile was purchased from Sigma-Aldrich in the highest available purity and used without any further purification. Ultrapure water (resistivity of 18.2 MΩ/cm at 25 °C) was produced in our laboratory by means of a Millipore Milli-Q system. Chromatographic separation was performed on a reverse-phase Zorbax C8

https://doi.org/10.1021/acsomega.3c07034
ACS Omega 2023, 8, 45078−45087

column 4.6 × 150 mm, 5 μm (Agilent Technologies, CA, USA), at a flow rate of 0.5 mL/min, with the linear gradient H_2O (HCOOH 0.1%)/CH_3CN from 20:80 to 5:95.

MS/MS (ESI+) parameters: DHA-s-UDCMe precursor ion 795 [M + 23], product ion 261, cen 43 eV.

4.3. Biological Evaluation. *4.3.1. Cell Culture and Treatments.* African green monkey epithelial kidney cells, VERO C1008 (Vero E6, ATCC CRL1586TM) and human epithelial lung cells Calu-3 (ATCC HTB-55) were grown in Eagle's minimal essential medium (MEM) with nonessential amino acids (Lonza Biosciences) supplemented with 10% heat-inactivated fetal calf serum (FCS, Gibco), penicillin−streptomycin mixture (1X, Gibco), and L-glutamine (2 mM; Lonza Biosciences). Cells were maintained at 37 °C in a humidified atmosphere with 5% CO_2.

Cells were treated with DHA, UDCA or conjugates at the following concentrations: 1, 10, 20, 40, and 80 μM for the viability assay. In order to test the antiviral activity, a time-of-drug addition was performed by adding molecules 1 h before, during, or after infection.

4.3.2. MTT Assay for Cell Viability. Cell viability was determined by the MTT (3-(4,5-dimethilthiazol-2yl)-2,5-diphenyl tetrazolium bromide) colorimetric assay (Roche Diagnostics Corporation, Indianapolis, IN, USA) following the manufacturer's instructions. Cells were treated with different concentrations of conjugates for 24 h, and viability was determined by absorbance reading at 570 nm.

4.3.3. SARS-CoV-2 Propagation and Infection. A SARS-CoV-2 inoculum was isolated from a nasopharyngeal swab of a COVID-19 patient (Caucasian man of Italian origin; genome sequences available at GenBank (SARS-CoV-2-UNIBS-AP66: ERR4145453)) and was a kind gift of Professor Arnaldo Caruso (University of Brescia, Italy). SARS-CoV-2 was propagated in Vero E6 cells and titrated by the plaque assay as described previously.[48] Both Vero E6 and Calu-3 were infected with an MOI of 0.1 for 2 h at 37 °C, as previously reported.[49] An hour after infection, the supernatants of infected cells were collected. All procedures were carried out in a biosafety level-3 (BSL-3) laboratory.

4.3.4. Antiviral Activity Evaluation. RNA was extracted from 500 μL of clarified cell culture supernatants (16,000*g* × 10 min) using a PureLink Viral RNA/DNA Mini Kit (Thermo Fisher, Milan, Italy) according to the manufacturer's instructions. RNA was eluted in 15 μL of RNase-free water and stored at −80 °C until use. RNA was then reverse transcripted with SuperScript IV VILO (Thermo Fisher, Milan, Italy). Sars-CoV-2 genomes were quantified by amplification of the S gene using a PowerUp SYBR Green Master Mix (Thermo Fisher, Milan, Italy) with the following primers: RBD-qF1:5′-AATGGTTTAACAGGCACAGG-3′ and RBD-qR1:5′-CTCAAGTGTCTGTGGATCACG-3. For absolute quantification, a dsDNA fragment (gBlock, Integrated DNA Technologies, Coralville, IA, USA) based on the RBD sequence was used to generate a standard curve ranging from 10^8 to 10^2 copies.

The plaque assay was used to determine the levels of infective SARS-CoV-2 released by treated cells. Briefly, supernatants derived from treated infected Calu-3 cells were used to infect Vero E6. Five days after infection, cells were methanol-fixed, and plaques were stained with crystal violet (0.1%) and counted. The experiments were performed in triplicate.

4.3.5. ACE2 Gene Expression Analysis. Ace2 gene expression was evaluated on total RNA extracted from cells after 48 hpi using a PureLink RNA Mini Kit (Invitrogen, Waltham, MA, USA), and DNase treatment was used to check for contaminant DNA presence using β-actin PCR as a control. An RT2 first strand kit (Qiagen, Milan, Italy) was used for RNA reverse transcription, and cDNAs were immediately used or stored at −20 °C. Gene expression analysis on extracted RNA was performed by real-time quantitative PCR using a PowerUp SYBR Green Master Mix (Thermo Fisher, Milan, Italy) with the following primer sets: GAPDH (Hs.PT.58.25887499.g) and ACE2 (Hs.PT.58.27645939). Relative quantification of mRNA levels for the samples was calculated using the $2^{-\Delta\Delta CT}$ method, normalized to the housekeeping gene GAPDH. For all experiments, at least three replicates were performed.

4.3.6. Immunofluorecence Assay. ACE2 protein expression in Calu-3 cell lines was evaluated by incubation with a specific antibody against human angiotensin-converting enzyme 2 (ACE2) (SN0754 Thermo Fisher; Italy) as previously described[50] followed by incubation with the FITC goat antimouse IgG (H + L) secondary antibody (Thermo Fisher, Milan, Italy). Immunofluorescence was visualized by fluorescence microscopy (Nikon Eclipse TE2000S, Milan, Italy). DNA was stained using DAPI (Thermo Fisher, Milan, Italy).

■ ASSOCIATED CONTENT

Supporting Information

The Supporting Information is available free of charge at https://pubs.acs.org/doi/10.1021/acsomega.3c07034.

Cytotoxicity evaluation of hybrids DHA-UDC, DHA-t-UDCMe, and DHA-s-UDCMe; evaluation of antiviral activity of hybrid DHA-UDC; spectroscopic data of compounds 3β-Br-UDCMe, DHA-t-UDCMe, DHA-UDC, and DHA-s-UDCMe (PDF)

■ AUTHOR INFORMATION

Corresponding Authors

Daniela Perrone − *Department of Environmental and Prevention Sciences, University of Ferrara, 44121 Ferrara, Italy*; Email: daniela.perrone@unife.it

Maria Luisa Navacchia − *Institute for Organic Synthesis and Photoreactivity (ISOF), National Research Council of Italy (CNR), I-40129 Bologna, Italy*; orcid.org/0000-0001-7175-1504; Email: marialuisa.navacchia@isof.cnr.it

Authors

Elena Marchesi − *Department of Environmental and Prevention Sciences, University of Ferrara, 44121 Ferrara, Italy*

Valentina Gentili − *Department of Chemical, Pharmaceutical and Agricultural Sciences, University of Ferrara, 44121 Ferrara, Italy*

Daria Bortolotti − *Department of Chemical, Pharmaceutical and Agricultural Sciences, University of Ferrara, 44121 Ferrara, Italy*

Lorenzo Preti − *Department of Chemical, Pharmaceutical and Agricultural Sciences, University of Ferrara, 44121 Ferrara, Italy*

Paolo Marchetti − *Department of Chemical, Pharmaceutical and Agricultural Sciences, University of Ferrara, 44121 Ferrara, Italy*

https://doi.org/10.1021/acsomega.3c07034
ACS Omega 2023, 8, 45078−45087

Virginia Cristofori − *Department of Chemical, Pharmaceutical and Agricultural Sciences, University of Ferrara, 44121 Ferrara, Italy;* orcid.org/0000-0002-6837-6042

Anna Fantinati − *Department of Environmental and Prevention Sciences, University of Ferrara, 44121 Ferrara, Italy*

Roberta Rizzo − *Department of Chemical, Pharmaceutical and Agricultural Sciences, University of Ferrara, 44121 Ferrara, Italy*

Claudio Trapella − *Department of Chemical, Pharmaceutical and Agricultural Sciences, University of Ferrara, 44121 Ferrara, Italy*

Complete contact information is available at: https://pubs.acs.org/10.1021/acsomega.3c07034

Author Contributions

#E.M. and V.G. are co-first authors.

Author Contributions

∇D.P. and M.L.N. are co-last authors.

Author Contributions

M.L.N., D.P., R.R., C.T., and P.M. performed conceptualization; M.L.N. and D.P. performed supervision; V.G., D.B., and M.L.N. performed formal analysis; E.M., V.G., L.P., D.B., V.C., and A.F. performed investigation; M.L.N., D.P., and D.B. performed original draft preparation; M.L.N., D.P., D.B., C.T., R.R., and P.M. reviewed and edited the manuscript.

Notes

The authors declare no competing financial interest.

■ ACKNOWLEDGMENTS

We gratefully acknowledge the University of Ferrara (fondi FAR) for financial support. Thanks are also given to Paolo Formaglio for NMR experiments and Marco Carmosino for technical assistance.

■ REFERENCES

(1) *COVID-19 Weekly Epidemiological Update, Edition 112*; (Accessed October 17, 2022). https://apps.who.int/iris/handle/10665/363395.

(2) Wang, C.; Yu, C.; Jing, H.; Wu, X.; Novakovic, V. A.; Xie, R.; Shi, J. Long COVID: The Nature of Thrombotic Sequelae Determines the Necessity of Early Anticoagulation. *Front. Cell. Infect. Microbiol.* **2022**, *12*, No. 861703, DOI: 10.3389/fcimb.2022.861703.

(3) Zamboni, P.; Bortolotti, D.; Occhionorelli, S.; Traina, L.; Neri, L. M.; Rizzo, R.; Gafâ, R.; Passaro, A. Bowel Ischemia as Onset of COVID-19 in Otherwise Asymptomatic Patients with Persistently Negative Swab. *J. Int. Med.* **2022**, *291* (2), 224−231.

(4) Mehandru, S.; Merad, M. Pathological Sequelae of Long-Haul COVID. *Nat. Immunol.* **2022**, *23* (2), 194−202.

(5) Bortolotti, D.; Simioni, C.; Neri, L. M.; Rizzo, R.; Semprini, C. M.; Occhionorelli, S.; Laface, I.; Sanz, J. M.; Schiuma, G.; Rizzo, S.; Varano, G.; Beltrami, S.; Gentili, V.; Gafâ, R.; Passaro, A. Relevance of VEGF and CD147 in Different SARS-CoV-2 Positive Digestive Tracts Characterized by Thrombotic Damage. *FASEB J.* **2021**, *35* (12), No. e21969, DOI: 10.1096/fj.202100821RRR.

(6) Bermejo, J. A. P.; Kang, S.; Rockwood, S. J.; Simoneau, C. R.; Joy, D. A.; Silva, A. C.; Ramadoss, G. N.; Flanigan, W. R.; Fozouni, P.; Li, H.; Chen, P. Y.; Nakamura, K.; Whitman, J. D.; Hanson, P. J.; McManus, B. M.; Ott, M.; Conklin, B. R.; McDevitt, T. C. SARS-CoV-2 Infection of Human IPSC Derived Cardiac Cells Reflects Cytopathic Features in Hearts of Patients with COVID-19. *Sci. Transl. Med.* **2021**, *13* (590), 1−16.

(7) Repurposed Antiviral Drugs for Covid-19 — Interim WHO Solidarity Trial Results. *N. Engl. J. Med.* **2021**, *384* (6), 497−511. .

(8) *COVID-19 Treatment Guidelines*; (Accessed October 17, 2022). https://www.covid19treatmentguidelines.nih.gov.

(9) Gambino, D. Editorial: Development/Repurposing of Drugs to Tackle the Multiple Variants of SARS-CoV- 2. *Front. Drug Discovery* **2023**, *3*, No. 1157688.

(10) Atanasov, A. G.; Zotchev, S. B.; Dirsch, V. M.; Orhan, I. E.; Banach, M.; Rollinger, J. M.; Barreca, D.; Weckwerth, W.; Bauer, R.; Bayer, E. A.; Majeed, M.; Bishayee, A.; Bochkov, V.; Bonn, G. K.; Braidy, N.; Bucar, F.; Cifuentes, A.; D'Onofrio, G.; Bodkin, M.; Diederich, M.; Dinkova-Kostova, A. T.; Efferth, T.; El Bairi, K.; Arkells, N.; Fan, T. P.; Fiebich, B. L.; Freissmuth, M.; Georgiev, M. I.; Gibbons, S.; Godfrey, K. M.; Gruber, C. W.; Heer, J.; Huber, L. A.; Ibanez, E.; Kijjoa, A.; Kiss, A. K.; Lu, A.; Macias, F. A.; Miller, M. J. S.; Mocan, A.; Müller, R.; Nicoletti, F.; Perry, G.; Pittalà, V.; Rastrelli, L.; Ristow, M.; Russo, G. L.; Silva, A. S.; Schuster, D.; Sheridan, H.; Skalicka-Woźniak, K.; Skaltsounis, L.; Sobarzo-Sánchez, E.; Bredt, D. S.; Stuppner, H.; Sureda, A.; Tzvetkov, N. T.; Vacca, R. A.; Aggarwal, B. B.; Battino, M.; Giampieri, F.; Wink, M.; Wolfender, J. L.; Xiao, J.; Yeung, A. W. K.; Lizard, G.; Popp, M. A.; Heinrich, M.; Berindan-Neagoe, I.; Stadler, M.; Daglia, M.; Verpoorte, R.; Supuran, C. T. Natural Products in Drug Discovery: Advances and Opportunities. *Nat. Rev. Drug Discovery* **2021**, *20* (3), 200−216.

(11) Tu, Y. The Discovery of Artemisinin (Qinghaosu) and Gifts from Chinese Medicine. *Nat. Med.* **2011**, *17* (10), 1217−1220.

(12) Ma, Z.; Woon, C. Y. N.; Liu, C. G.; Cheng, J. T.; You, M.; Sethi, G.; Wong, A. L. A.; Ho, P. C. L.; Zhang, D.; Ong, P.; Wang, L.; Goh, B. C. Repurposing Artemisinin and Its Derivatives as Anticancer Drugs: A Chance or Challenge? *Front. Pharmacol.* **2021**, *12*, No. 828856.

(13) Wong, Y. K.; Xu, C.; Kalesh, K. A.; He, Y.; Lin, Q.; Wong, W. S. F.; Shen, H. M.; Wang, J. Artemisinin as an Anticancer Drug: Recent Advances in Target Profiling and Mechanisms of Action. *Med. Res. Rev.* **2017**, *37* (6), 1492−1517.

(14) Efferth, T. Willmar Schwabe Award 2006: Antiplasmodial and Antitumor Activity of Artemisinin - From Bench to Bedside. *Planta Med.* **2007**, *73* (4), 299−309.

(15) Oiknine-Djian, E.; Weisblum, Y.; Panet, A.; Wong, H. N.; Haynes, R. K.; Wolf, D. G. The Artemisinin Derivative Artemisone Is a Potent Inhibitor of Human Cytomegalovirus Replication. *Antimicrob. Agents Chemother.* **2018**, *62* (7), No. e00288-18.

(16) Han, Y.; Pham, H. T.; Xu, H.; Quan, Y.; Mesplède, T. Antimalarial Drugs and Their Metabolites Are Potent Zika Virus Inhibitors. *J. Med. Virol.* **2019**, *91* (7), 1182−1190.

(17) Farmanpour-Kalalagh, K.; Beyraghdar Kashkooli, A.; Babaei, A.; Rezaei, A.; van der Krol, A. R. Artemisinins in Combating Viral Infections Like SARS-CoV-2, Inflammation and Cancers and Options to Meet Increased Global Demand. *Front. Plant Sci.* **2022**, *13*, No. 780257.

(18) Cao, R.; Hu, H.; Li, Y.; Wang, X.; Xu, M.; Liu, J.; Zhang, H.; Yan, Y.; Zhao, L.; Li, W.; Zhang, T.; Xiao, D.; Guo, X.; Li, Y.; Yang, J.; Hu, Z.; Wang, M.; Zhong, W. Anti-SARS-CoV-2 Potential of Artemisinins in Vitro. *ACS Infect. Dis.* **2020**, *6* (9), 2524−2531.

(19) Soni, R.; Shankar, G.; Mukhopadhyay, P.; Gupta, V. A Concise Review on Artemisia Annua L.: A Major Source of Diverse Medicinal Compounds. *Ind. Crops Prod.* **2022**, *184* (May), 115072.

(20) Gendrot, M.; Duflot, I.; Boxberger, M.; Delandre, O.; Jardot, P.; Le Bideau, M.; Andreani, J.; Fonta, I.; Mosnier, J.; Rolland, C.; Hutter, S.; La Scola, B.; Pradines, B. Antimalarial Artemisinin-Based Combination Therapies (ACT) and COVID-19 in Africa: In Vitro Inhibition of SARS-CoV-2 Replication by Mefloquine-Artesunate. *Int. J. Infect. Dis.* **2020**, *99* (December 2019), 437−440.

(21) Marchesi, E.; Perrone, D.; Navacchia, M. L. Molecular Hybridization as a Strategy for Developing Artemisinin-Derived Anticancer Candidates. *Pharmaceutics* **2023**, *15*, 2185.

(22) Çapcı, A.; Lorion, M. M.; Wang, H.; Simon, N.; Leidenberger, M.; Borges Silva, M. C.; Moreira, D. R. M.; Zhu, Y.; Meng, Y.; Chen, J. Y.; Lee, Y. M.; Friedrich, O.; Kappes, B.; Wang, J.; Ackermann, L.;

Tsogoeva, S. B. Artemisinin−(Iso)Quinoline Hybrids by C−H Activation and Click Chemistry: Combating Multidrug-Resistant Malaria. *Angew. Chemie - Int. Ed.* **2019**, *58* (37), 13066−13079.
(23) Frohlich, T.; Karagoz, A. Ç.; Reiter, C.; Tsogoeva, S. B. Artemisinin-Derived Dimers: Potent Antimalarial and Anticancer Agents. *J. Med. Chem.* **2016**, *59* (16), 7360−7388.
(24) Meunier, B. Hybrid Molecules with a Dual Mode of Action: Dream or Reality? *Acc. Chem. Res.* **2008**, *41* (1), 69−77.
(25) Zimmermann, G. R.; Lehár, J.; Keith, C. T. Multi-Target Therapeutics: When the Whole Is Greater than the Sum of the Parts. *Drug Discovery Today* **2007**, *12* (1−2), 34−42.
(26) Fiorucci, S.; Distrutti, E. The Pharmacology of Bile Acids and Their Receptors. *Handb. Exp. Pharmacol.* **2019**, *256*, 3−18.
(27) Li, T.; Chiang, J. Y. L. Bile Acid Signaling in Metabolic Disease and Drug Therapy. *Pharmacol. Rev.* **2014**, *66* (4), 948−983.
(28) Copple, B. L.; Li, T. Pharmacology of Bile Acid Receptors: Evolution of Bile Acids from Simple Detergents to Complex Signaling Molecules. *Pharmacol. Res.* **2016**, *104*, 9−21.
(29) Brevini, T.; Maes, M.; Webb, G. J.; John, B. V.; Fuchs, C. D.; Buescher, G.; Wang, L.; Griffiths, C.; Brown, M. L.; Scott, W. E.; Pereyra-Gerber, P.; Gelson, W. T. H.; Brown, S.; Dillon, S.; Muraro, D.; Sharp, J.; Neary, M.; Box, H.; Tatham, L.; Stewart, J.; Curley, P.; Pertinez, H.; Forrest, S.; Mlcochova, P.; Varankar, S. S.; Darvish-Damavandi, M.; Mulcahy, V. L.; Kuc, R. E.; Williams, T. L.; Heslop, J. A.; Rossetti, D.; Tysoe, O. C.; Galanakis, V.; Vila-Gonzalez, M.; Crozier, T. W. M.; Bargehr, J.; Sinha, S.; Upponi, S. S.; Fear, C.; Swift, L.; Saeb-Parsy, K.; Davies, S. E.; Wester, A.; Hagström, H.; Melum, E.; Clements, D.; Humphreys, P.; Herriott, J.; Kijak, E.; Cox, H.; Bramwell, C.; Valentijn, A.; Illingworth, C. J. R.; Dahman, B.; Bastaich, D. R.; Ferreira, R. D.; Marjot, T.; Barnes, E.; Moon, A. M.; Barritt, A. S.; Gupta, R. K.; Baker, S.; Davenport, A. P.; Corbett, G.; Gorgoulis, V. G.; Buczacki, S. J. A.; Lee, J. H.; Matheson, N. J.; Trauner, M.; Fisher, A. J.; Gibbs, P.; Butler, A. J.; Watson, C. J. E.; Mells, G. F.; Dougan, G.; Owen, A.; Lohse, A. W.; Vallier, L.; Sampaziotis, F. FXR Inhibition May Protect from SARS-CoV-2 Infection by Reducing ACE2. *Nature* **2023**, *615* (7950), 134−142.
(30) Thuy, P. X.; Bao, T. D. D.; Moon, E. Y. Ursodeoxycholic Acid Ameliorates Cell Migration Retarded by the SARS-CoV-2 Spike Protein in BEAS-2B Human Bronchial Epithelial Cells. *Biomed. Pharmacother.* **2022**, *150* (April), 113021.
(31) *The Application of Ursodeoxycholic Acid for the Prevention of SARS-CoV-2 Infection (COVID-19)*; ClinicalTrials.Gov Identifier: NCT05659654.
(32) Marchesi, E.; Chinaglia, N.; Capobianco, M. L.; Marchetti, P.; Huang, T. E.; Weng, H. C.; Guh, J. H.; Hsu, L. C.; Perrone, D.; Navacchia, M. L. Dihydroartemisinin−Bile Acid Hybridization as an Effective Approach to Enhance Dihydroartemisinin Anticancer Activity. *ChemMedChem.* **2019**, *14* (7), 779−787.
(33) Huang, T. E.; Deng, Y. N.; Hsu, J. L.; Leu, W. J.; Marchesi, E.; Capobianco, M. L.; Marchetti, P.; Navacchia, M. L.; Guh, J. H.; Perrone, D.; Hsu, L. C. Evaluation of the Anticancer Activity of a Bile Acid-Dihydroartemisinin Hybrid Ursodeoxycholic-Dihydroartemisinin in Hepatocellular Carcinoma Cells. *Front. Pharmacol.* **2020**, *11*, No. 599067.
(34) Hsu, Y. F.; Kung, F. L.; Huang, T. E.; Deng, Y. N.; Guh, J. H.; Marchetti, P.; Marchesi, E.; Perrone, D.; Navacchia, M. L.; Hsu, L. C. Anticancer Activity and Molecular Mechanisms of an Ursodeoxycholic Acid Methyl Ester-Dihydroartemisinin Hybrid via a Triazole Linkage in Hepatocellular Carcinoma Cells. *Molecules* **2023**, *28* (5), 2358 DOI: 10.3390/molecules28052358.
(35) Bakouny, Z.; Hawley, J. E.; Choueiri, T. K.; Peters, S.; Rini, B. I.; Warner, J. L.; Painter, C. A. COVID-19 and Cancer: Current Challenges and Perspectives. *Cancer Cell* **2020**, *38* (5), 629−646.
(36) Bora, V. R.; Patel, B. M. The Deadly Duo of COVID-19 and Cancer! *Front. Mol. Biosci.* **2021**, *8*, No. 643004, DOI: 10.3389/fmolb.2021.643004.
(37) Saini, G.; Aneja, R. Cancer as a Prospective Sequela of Long COVID-19. *BioEssays* **2021**, *43* (6), 1−5.
(38) Herrmann, L.; Yaremenko, I. A.; Çapcı, A.; Struwe, J.; Tailor, D.; Dheeraj, A.; Hodek, J.; Belyakova, Y. Y.; Radulov, P. S.; Weber, J.; Malhotra, S. V.; Terent'ev, A. O.; Ackermann, L.; Tsogoeva, S. B. Synthesis and in Vitro Study of Artemisinin/Synthetic Peroxide-Based Hybrid Compounds against SARS-CoV-2 and Cancer. *ChemMedChem.* **2022**, *17* (9), 1−6.
(39) Perrone, D.; Bortolini, O.; Fogagnolo, M.; Marchesi, E.; Mari, L.; Massarenti, C.; Navacchia, M. L.; Sforza, F.; Varani, K.; Capobianco, M. L. Synthesis and in Vitro Cytotoxicity of Deoxyadenosine−Bile Acid Conjugates Linked with 1,2,3-Triazole. *New J. Chem.* **2013**, *37* (11), 3559−3567.
(40) Massarenti, C.; Bortolini, O.; Fantin, G.; Cristofaro, D.; Ragno, D.; Perrone, D.; Marchesi, E.; Toniolo, G.; Massi, A. Fluorous-Tag Assisted Synthesis of Bile Acid-Bisphosphonate Conjugates: Via Orthogonal Click Reactions: An Access to Potential Anti-Resorption Bone Drugs. *Org. Biomol. Chem.* **2017**, *15* (22), 4907−4920.
(41) Batesky, D. C.; Goldfogel, M. J.; Weix, D. J. Removal of Triphenylphosphine Oxide by Precipitation with Zinc Chloride in Polar Solvents. *J. Org. Chem.* **2017**, *82* (19), 9931−9936.
(42) Kapkoti, D. S.; Singh, S.; Luqman, S.; Bhakuni, R. S. Synthesis of Novel 1,2,3-Triazole Based Artemisinin Derivatives and Their Antiproliferative Activity. *New J. Chem.* **2018**, *42*, 5978−5995.
(43) Parapini, S.; Olliaro, P.; Navaratnam, V.; Taramelli, D.; Basilico, N. Stability of the Antimalarial Drug Dihydroartemisinin under Physiologically Relevant Conditions: Implications for Clinical Treatment and Pharmacokinetic and in Vitro Assays. *Antimicrob. Agents Chemother.* **2015**, *59* (7), 4046−4052.
(44) Jefford, C. W.; Vicente, M. G. H.; Jacquier, Y.; Favarger, F.; Mareda, J.; Millasson-Schmidt, P.; Brunner, G.; Burger, U. The Deoxygenation and Isomerization of Artemisinin and Artemether and Their Relevance to Antimalarial Action. *Helv. Chim. Acta* **1996**, *79* (5), 1475−1487.
(45) Presser, A.; Feichtinger, A.; Buzzi, S. A Simplified and Scalable Synthesis of Artesunate. *Monatshefte fur Chemie* **2017**, *148* (1), 63−68.
(46) Pires De Souza, G. A.; Le Bideau, M.; Boschi, C.; Wurtz, N.; Colson, P.; Aherfi, S.; Devaux, C.; La Scola, B. Choosing a Cellular Model to Study SARS-CoV-2. *Front. Cell. Infect. Microbiol.* **2022**, *12*, No. 1003608.
(47) Xu, Z.; Zhao, S. J.; Liu, Y. 1,2,3-Triazole-Containing Hybrids as Potential Anticancer Agents: Current Developments, Action Mechanisms and Structure-Activity Relationships. *Eur. J. Med. Chem.* **2019**, *183*, 111700.
(48) Caccuri, F.; Messali, S.; Bortolotti, D.; Di Silvestre, D.; De Palma, A.; Cattaneo, C.; Bertelli, A.; Zani, A.; Milanesi, M.; Giovanetti, M.; Campisi, G.; Gentili, V.; Bugatti, A.; Filippini, F.; Scaltriti, E.; Pongolini, S.; Tucci, A.; Fiorentini, S.; D'Ursi, P.; Ciccozzi, M.; Mauri, P.; Rizzo, R.; Caruso, A. Competition for Dominance within Replicating Quasispecies during Prolonged SARS-CoV-2 Infection in an Immunocompromised Host. *Virus Evol.* **2022**, *8* (1), veac042 DOI: 10.1093/ve/veac042.
(49) Gentili, V.; Pazzi, D.; Rizzo, S.; Schiuma, G.; Marchini, E.; Papadia, S.; Sartorel, A.; Di Luca, D.; Caccuri, F.; Bignozzi, C. A.; Rizzo, R. Transparent Polymeric Formulations Effective against SARS-CoV-2 Infection. *ACS Appl. Mater. Interfaces* **2021**, *13* (46), 54648−54655.
(50) Bortolotti, D.; Gentili, V.; Rizzo, S.; Schiuma, G.; Beltrami, S.; Strazzabosco, G.; Fernandez, M.; Caccuri, F.; Caruso, A.; Rizzo, R. Tlr3 and Tlr7 Rna Sensor Activation during Sars-Cov-2 Infection. *Microorganisms* **2021**, *9* (9). 1820.

https://doi.org/10.1021/acsomega.3c07034
ACS Omega 2023, 8, 45078−45087